A SIMPLE EM MODEL FOR DETERMINING THE SCATTERED MAGNETIC RESONANCE RADIOFREQUENCY FIELD OF AN IMPLANTED MEDICAL DEVICE

S. A. Mohsin

University of Engineering and Technology
Lahore, Pakistan

Abstract—A radiofrequency field (RF) field exists inside body tissue during magnetic resonance imaging (MRI). If any implanted medical device is present, there can be a very intense concentration of the scattered RF field in the tissue surrounding certain parts of the implant. This causes tissue heating that can reach dangerous levels. Scattered field considerations show that it is possible to neglect the loading effect of the implant on the MR RF source. This leads to an incident field simplification. The presence of the implant in nonhomogeneous tissue increases the complexity of the scattering problem. An approach is presented that makes the computational problem considerably smaller. A method of moments (MoM) formulation of the EM model is presented. The relevant issues that arise during a finite element method (FEM) formulation are also discussed. The methods are illustrated by solving the problem for typical implants using MoM as well as FEM.

1. INTRODUCTION

During MRI, three types of fields are used. Two of the fields, a uniform and static magnetic field, and low frequency gradient magnetic fields do not pose a heating risk, but the third field, the RF field, poses a significant heating risk inside body tissues. The source of the RF field is a coil, usually called a birdrcage coil, since it encloses the MRI chamber. The incident RF field is that which exists inside the chamber in the absence of body tissue. When body tissue is present inside the chamber, a scattered field is produced and the total field at any point inside the chamber (inside tissue or in air) is the sum

---

of the scattered and incident fields. The loading effect of body tissue on the RF source cannot be neglected and a computational domain will include the chamber and the RF coil conductors. The scattered field is concentrated in some parts of the body and there is some heating due to the flow of conduction currents, but this heating is much below hazardous levels [1, 2]. When one or more implanted medical devices such as deep brain stimulation (DBS) leads, other lead devices, pacemakers, stents, artificial bone or bone support implants, etc. [3–5], are present inside tissue, an additional scattered field is produced. This scattered field can be very concentrated in the tissue surrounding the implant or certain parts of it [6]. The resulting heating, though limited to small tissue regions can be very hazardous [7, 8]. An exact scattering formulation will involve integrations over the the entire tissue region, the implant, as well as surface integrations over the conductors of the surrounding MR birdcage coil. The scattered field, though, decays very rapidly with distance as we move away from the implant [9]. Thus the loading affect of the implant on the MR coil (the actual MR RF source) can be neglected. Therefore, the RF field that exists inside tissue in the absence of any implant needs to be computed first. This computed field can then be used as the incident field when an implant is present. The problem of an implant embedded in nonhomogeneous tissue can then be investigated. In the present paper, a simple electromagnetic (EM) model for the problem is developed and a MoM formulation based on this simplified approach is presented. The issues that arise during a FEM formulation are also addressed. It should be noted that a simplified (general) approach for determining the scattered MR RF field of any implant is developed here; the approach is not restricted to a particular kind of implant. For validation, the approach has been used for computing the scattered fields and induced temperature rises of two different implants in Section 4. Computations are made with both MoM and FEM and the computed results are also compared with measurements made in the laboratory.

2. THE INCIDENT AND THE SCATTERED FIELDS

Consider body tissue inside a MR coil *with no implant present*. The total field $(\mathbf{E}, \mathbf{H})$ at any point must satisfy

$$\left.\begin{array}{l} \vec{\nabla} \times \mathbf{H} = \mathbf{J} + j\omega\varepsilon_o\mathbf{E} \\ \vec{\nabla} \times \mathbf{E} = -j\omega\mu_o\mathbf{H} \end{array}\right\} \tag{1}$$

where in air $\mathbf{J} = 0$, over the MR RF source (i.e., the MR coil) $\mathbf{J}$ is the source current density, and in tissue $\mathbf{J} = [\sigma + j\omega(\varepsilon - \varepsilon_o)]\,\mathbf{E}$ where the tissue conductivity σ and permittivity ε are functions of

position. The field $(\mathbf{E}, \mathbf{H})$ may be computed by employing a suitable numerical method such as the Finite Difference Time Domain (FDTD) method [10]. It should be noted here that the loading effect of body tissue on the MR RF source must be considered and is part of the computation.

Now consider an implant embedded in tissue. In an ideal analysis, we should consider the whole system again and find the field $(\mathbf{E}, \mathbf{H})$ at any point satisfying the Maxwell's Equations (1); the only difference is that the implant embedded in tissue occupies a volume V^I in which $\mathbf{J} = [\sigma_I + j\omega(\varepsilon_I - \varepsilon_o)] \mathbf{E}$, where σ_I is the conductivity and ε_I the permittivity of the implant material (these take on different values over the implant structure). This whole computation would be very expensive indeed (see Section 3). Some a-priori considerations can lead to simplified approach and the resulting computation will be far less expensive. We now discuss these considerations.

The scattered field of an implant becomes small 3–5 cm away from the implant [9, 11]. Let d be the distance from an observation point to the nearest point on the implant structure. We define d_o as that minimum value of d at which the scattered field can be considered as having become negligible. Negligible here means that the total electric field is within a few volts per meter of the background electric field, where the background field is that field that exists in body tissue during MRI in the *absence of any medical implant (s)*. This consideration can be from a source perspective, that is, the equivalent source current density produced in tissue, $\mathbf{J} = [\sigma + j\omega(\varepsilon - \varepsilon_o)] \mathbf{E}$, is small. From a practical perspective, $\mathbf{J}$ of a significant strength will exist only at points in the vicinity of the implant. For most implants, a value of d_o in the range 3–5 cm will suffice. As we move in tissue around the implant structure, the value of d_o will depend upon:

- the specific part of the implant to which this distance d_o is measured. For example, d_o will be comparatively larger around the electrodes of a DBS lead implant than around the connecting part of the lead. Other examples of parts of implants around which d_o is larger than the rest of the implant structure are: protruding metal tip of a long insulated lead implant, tip of a steel pin in a bone support frame, round metal end of an artificial hip joint, and the ends of a stent.
- the type and nature of the overall implant structure.
- the tissue composition. For example fat is less dissipative (lossy) than muscle tissue.

We now explain why it is often possible to assume tissue as a medium infinite in extent for implant scattering. The air-tissue interface effect

is actually quite small and for implants at an implantation depth of 1 cm or more it is negligible. Even when the implant is embedded just below the skin (e.g., DBS lead implants), the air-tissue interface effect is still very small [9]. The fact that an implant may not lie near the interface along the implant's entire length or extent further lessens the interface effect. For most practical cases, the air-tissue interface effect can be safely neglected, and the implant can be considered as being embedded in tissue that extends to infinity in all directions.

The considerations discussed above lead us to the conclusion that the loading effect of the implant on the MR RF source (the birdcage coil) is negligible and the *total RF field* ($\mathbf{E}$, $\mathbf{H}$) *that exists in tissue in the absence of any implant can be set equal to the incident field* ($\mathbf{E}^i$, $\mathbf{H}^i$) *where* ($\mathbf{E}^i$, $\mathbf{H}^i$) *is taken to be the incident field that excites the implant structure embedded in tissue.*

Tissue is nonhomogeneous in nature. Since as discussed above, d_o is small, the nonhomogeneous nature of tissue will matter in the only in the vicinity of the implant. We only need to consider a nonhomogeneous tissue layer having thickness d_o completely surrounding the implant structure (and, touching the implant's exterior surface). For further reduction in the size of the computation, the thickness of the encompassing nonhomogeneous tissue layer can be taken as $d_o/2$ or $d_o/4$, or even smaller. The rest of the tissue, called background tissue here, extends to infinity in all outward directions and has the constitutive parameters of average body tissue. We specify the constitutive parameters of the various sub-regions as:

- σ_I is the conductivity and ε_I the permittivity of the implant material occupying the volume V^I (these assume different values in the different material parts constituting the implant).

- σ is the conductivity and ε the permittivity of the nonhomogeneous tissue surrounding the implant. This occupies a volume, V^t. Note that σ and ε are functions of position in V^t.

- σ_b is the conductivity and ε_b the permittivity of the background tissue, occupying volume, V^b. Note that σ_b and ε_b are *not* functions of position in V^b and that V^b extends to infinity in all outward directions.

The scattered field ($\mathbf{E}^s$, $\mathbf{H}^s$) at any point then satisfies

$$\left. \begin{array}{l} \vec{\nabla} \times \mathbf{H}^s = \mathbf{J} + (\sigma_b + j\omega\varepsilon_b)\mathbf{E}^s \\ \vec{\nabla} \times \mathbf{E}^s = -j\omega\mu_o\mathbf{H}^s \end{array} \right\} \tag{2}$$

where

$$\mathbf{J} = [(\sigma_I - \sigma_b) + j\omega(\varepsilon_I - \varepsilon_b)]\, \mathbf{E}^s + [(\sigma_I - \sigma) + j\omega(\varepsilon_I - \varepsilon)]\; \mathbf{E}^i \text{ in } V^I \quad (3a)$$

$$\mathbf{J} = [(\sigma - \sigma_b) + j\omega(\varepsilon - \varepsilon_b)]\, \mathbf{E}^s \text{ in } V^t \quad (3b)$$

$$\mathbf{J} = 0 \text{ in } V^b \quad (3c)$$

Using the scattered vector magnetic potential $\mathbf{A}^s$, [12], we obtain the scattered RF electric field as

$$\mathbf{E}^s = -\frac{j}{\omega\mu_o} \frac{\vec{\nabla}(\vec{\nabla} \cdot \mathbf{A}^s)}{(\varepsilon_b - j\sigma_b/\omega)} - j\omega\mathbf{A}^s \quad (4)$$

3. COMPUTATIONAL METHODS

3.1. Discretization Using the Method of Moments

The discretization of the EM problem described by Eqs. (2) and (3) using the method of moments is presented here. Following the procedure outlined in [13], the formulation uses the Green's function of the wave equation for an infinite domain. Using Eq. (4), an operator $L(\mathbf{J})$ can be defined

$$L(\mathbf{J}) = -\mathbf{E}^s = \frac{j\vec{\nabla}(\vec{\nabla} \cdot \mathbf{A}^s)}{\omega\mu_O(\varepsilon_b - j\sigma_b/\omega)} + j\omega\mathbf{A}^s \quad (5)$$

where $\mathbf{A}^s$, the retarded vector magnetic potential, has the usual integral formulation over the volumes V^I and V^t (where $\mathbf{J}$ is nonzero). $\mathbf{J}$ is given by Eq. (3). Then we have from Eqs. (3) and (5)

$$L(\mathbf{J}) + \frac{\mathbf{J}}{(\sigma - \sigma_b) + j\omega(\varepsilon - \varepsilon_b)} = 0 \text{ in } V^t \quad (6)$$

$$L(\mathbf{J}) + \frac{\mathbf{J}}{(\sigma_I - \sigma_b) + j\omega(\varepsilon_I - \varepsilon_b)} = \frac{[(\sigma_I - \sigma) + j\omega(\varepsilon_I - \varepsilon)]\mathbf{E}^i}{(\sigma_I - \sigma_b) + j\omega(\varepsilon_I - \varepsilon_b)} \text{ in } V^I \quad (7)$$

For vector fields $\mathbf{u}$ and $\mathbf{v}$ we define an inner product as

$$\langle \mathbf{u}, \mathbf{v} \rangle_V = \int_V \mathbf{u} \cdot \mathbf{v}\, dV \quad (8)$$

over an appropriate volume V (which is $V^t \cup V^I$ here). The current density in V^t and V^I is expressed in terms of a summation of vector basis functions $\mathbf{J}_1, \mathbf{J}_2, \ldots, \mathbf{J}_N$

$$\mathbf{J} = \sum_{n=1}^{N} a_n\, \mathbf{J}_n \quad (9)$$

where the a_n are complex coefficients. We define vector testing functions $\mathbf{W_1}, \mathbf{W_2}, \ldots$ over V. Using Galerkin's procedure we can set $\mathbf{W}_m = \mathbf{J}_n, \ n = 1, 2, \ldots, N$. We note that $\langle \mathbf{W}_m, \mathbf{E}^s \rangle_V$ is a reaction [14, 15]. Applying the method of moments we obtain

$$\sum_{n=1}^{N} I_n \int_{V^t} \mathbf{W}_m \cdot \left[L(\mathbf{J}_n) + \frac{\mathbf{J}_n}{(\sigma - \sigma_b) + j\omega(\varepsilon - \varepsilon_b)} \right] dV$$

$$+ \sum_{n=1}^{N} I_n \int_{V^{\mathbf{I}}} \mathbf{W}_m \cdot \left[L(\mathbf{J}_n) + \frac{\mathbf{J}_n}{(\sigma_I - \sigma_b) + j\omega(\varepsilon_I - \varepsilon_b)} \right] dV$$

$$= \int_{V^{\mathbf{I}}} \mathbf{W}_m \cdot \frac{[(\sigma_I - \sigma) + j\omega(\varepsilon_I - \varepsilon)] \, \mathbf{E}^i \, dV}{(\sigma_I - \sigma_b) + j\omega(\varepsilon_I - \varepsilon_b)} \tag{10}$$

for all m and $L(\mathbf{J}_n)$ can be computed using the integral form for $\mathbf{A}^s$, and (5). Eq. (10) can be written as the matrix equation

$$\left[Z_{mn} + \hat{Z}_{mn} \right] [I_m] = [V_m] \tag{11}$$

where

$$[Z_{mn}] = \begin{bmatrix} \left\langle \mathbf{W}_1, L(\mathbf{J}_1) + \frac{\mathbf{J}_1}{\zeta_t} \right\rangle_{V^t} & \left\langle \mathbf{W}_1, L(\mathbf{J}_2) + \frac{\mathbf{J}_2}{\zeta_t} \right\rangle_{V^t} & \cdots \\ \left\langle \mathbf{W}_2, L(\mathbf{J}_1) + \frac{\mathbf{J}_1}{\zeta_t} \right\rangle_{V^t} & \left\langle \mathbf{W}_2, L(\mathbf{J}_2) + \frac{\mathbf{J}_2}{\zeta_t} \right\rangle_{V^t} & \cdots \\ \vdots & \vdots & \vdots \end{bmatrix}$$

the inner products in $[Z_{mn}]$ denoting integrations over V^t and

$$\zeta_t = \sigma - \sigma_b + j\omega(\varepsilon - \varepsilon_b)$$

$$[\hat{Z}_{mn}] = \begin{bmatrix} \left\langle \mathbf{W}_1, L(\mathbf{J}_1) + \frac{\mathbf{J}_1}{\zeta_I} \right\rangle_{V^{\mathbf{I}}} & \left\langle \mathbf{W}_1, L(\mathbf{J}_2) + \frac{\mathbf{J}_2}{\zeta_I} \right\rangle_{V^{\mathbf{I}}} & \cdots \\ \left\langle \mathbf{W}_2, L(\mathbf{J}_1) + \frac{\mathbf{J}_1}{\zeta_I} \right\rangle_{V^{\mathbf{I}}} & \left\langle \mathbf{W}_2, L(\mathbf{J}_2) + \frac{\mathbf{J}_2}{\zeta_I} \right\rangle_{V^{\mathbf{I}}} & \cdots \\ \vdots & \vdots & \vdots \end{bmatrix}$$

the inner products in $[\hat{Z}_{mn}]$ denoting integrations over V^I and

$$\zeta_I = \sigma_I - \sigma_b + j\omega(\varepsilon_I - \varepsilon_b)$$

$$[I_m] = \begin{bmatrix} a_1 \\ a_2 \\ \vdots \\ a_N \end{bmatrix} \qquad [V_m] = \begin{bmatrix} \langle \mathbf{W}_1, \mathbf{F} \rangle_{\mathbf{V^I}} \\ \langle \mathbf{W}_2, \mathbf{F} \rangle_{\mathbf{V^I}} \\ \vdots \\ \vdots \end{bmatrix}$$

the inner products in $[V_m]$ denoting integrations over V^I and

$$\mathbf{F} = \frac{\left[(\sigma_I - \sigma) + j\omega(\varepsilon_I - \varepsilon) \right] \mathbf{E}^i}{\zeta_I}$$

The solution is

$$\mathbf{J} = [\mathbf{J}_n][I_m] = [\mathbf{J}_n][Y_m][V_m] \tag{12}$$

where $[Y_m]$ is the inverse of the matrix $\left[Z_{mn} + \hat{Z}_{mn} \right]$.

3.2. Using the Finite Element Method

The size of the computational domain for FEM is finite and absorbing boundary conditions are enforced at the exterior boundaries. The FEM procedural details can be found in [16, 17]. Some of the pertinent issues regarding scattering by implants will be discussed here. Since for almost all implants, a value of d_o in the range 3–5 cm suffices (see Section 2), the FEM domain can be terminated at a distance of d_o from a point on the surface of the implant structure. In many implanted medical devices (e.g., lead implants, stents, artificial joints) the radial dimension is much smaller than the length [18]; for example, DBS leads have a diameter of about 1.5 mm but can be as long as 70 cm. For a reasonable analysis that gives meaningful results, the surface of the lead will have to be meshed very finely as compared to the rest of the domain. The nonhomogeneous tissue layer surrounding the lead (as discussed in Section 2) is the next in the priority of fine meshing. Parts of this tissue layer such as those surrounding the lead's electrodes need to be meshed more finely than the rest of the tissue. The background tissue, extending to the exterior boundaries of the domain, can be meshed less finely. Similar meshing considerations apply to parts of other implants (such as the tips of implanted steel pins in bone support frames, tips of implanted artificial joints, etc.) and the tissue immediately surrounding those parts. The very large number of elements required to finely mesh the implant structure can be as large or even larger than the number of elements used to mesh the rest of the domain This means that a computation over a large-sized domain (such as that containing all of the body tissue, air, and the MR birdcage coil, as mentioned in Section 2) in the *absence* of an implant would be much less expensive than in the *presence* of the implant.

4. RESULTS AND COMPARISONS

The computational methods presented in the present paper are applied to two different implants to demonstrate their applicability and

correctness. To demonstrate the robustness of the methods, a stent implant and a lead implant with four electrodes have been chosen. The computed results for these implants are compared to each other and to laboratory measurements as well. The implants merely serve as example implants to which the methods discussed in the paper can be applied; the emphasis is on the computational methods and not on the analysis of the example implants only. It is to be noted that the methods are perfectly general and can be applied to the MR RF scattering analysis of any implant.

Computations have been carried out on the two example implants in a 1.5 Tesla MR system. The MRI radiofrequency is 64 MHz. The first implant, a cylindrical stent, is 15 cm long and has a diameter of 8 mm. The stent has a thin plastic wall which contains a very finely woven metal wire mesh. At MRI RF frequencies, the capacitances between the thin wires short out the wires and the walls can be modeled as PEC (perfect electric conductor) surfaces; this suffices for an analysis covering the worst-case heating scenario. The second implant, a lead, consists of four insulated wires connecting a periodic pulse generator to four electrodes. The overall length of the lead (including the electrodes) is 25 cm. Each electrode is a solid metal cylinder, 1.27 mm in diameter and 1.5 mm long. The four electrodes are separated by insulation 1.5 mm thick. For each implant (considered separately), the scattered electric field is computed using MoM and the simplified EM model as described in Section 3.1. The scattered electric field is also found by applying FEM to the simplified EM model; the electric field wave equation is solved by employing the considerations outlined in Section 3.2. Comsol Multiphysics has been used as the partial differential equation solver. The heat equation, [6], is solved to find the temperature rises.

For the in-vitro temperature rise measurements, a phantom was placed inside an MRI RF coil. The phantom consisted of a salt solution (sodium chloride and polyacrylic acid partial sodium salt) with gel inside a plastic trough approximating the shape of the human body. The phantom was positioned so that landmark (center of the MRI RF coil) was well inside the phantom at the desired position. The MR RF input power was then adjusted such that:

- The background specific absorption rate (SAR), [6], was 2.10 W/kg at the landmark in phantom material with $\sigma = 0.27$ S/m and $\varepsilon_r = 77$. *Background SAR means that it is the SAR with no implant present in the phantom.* The stent was then placed inside the phantom such that its center (lengthwise) was at the landmark. The corresponding amplitude of the incident RF electric field at the landmark was 124.7 V/m.

- The background SAR was 2.35 W/kg at the landmark in phantom material with $\sigma = 0.47$ S/m and $\varepsilon_r = 80$. The lead was then placed inside the phantom such that its center (lengthwise) was at the landmark. The corresponding incident RF electric field at the landmark was 100 V/m.

The computations have been carried out to conform to this level of incident RF field excitation so that the computed and measured values can be directly compared without any scaling. The relationship between the background SAR at the landmark and the MRI input power is almost linear. The highest values of the incident RF electric field occur in fat tissue with $\sigma = 0.1$ S/m and $\varepsilon_r = 10$. For the given levels of the background SAR, the incident RF electric field (amplitude) values are 205 V/m (for the stent) and 216.8 V/m (for the lead).

The spatial electric field distribution obtained using the simplified FEM for the stent implant is shown in Fig. 1. The corresponding computed temperature rise distribution is shown in Fig. 2. Spatial distributions for the lead implant are shown in Figs. 3 and 4. The spatial distributions obtained using simplified MoM, and those obtained using the full MRI domain (full FEM) are essentially the
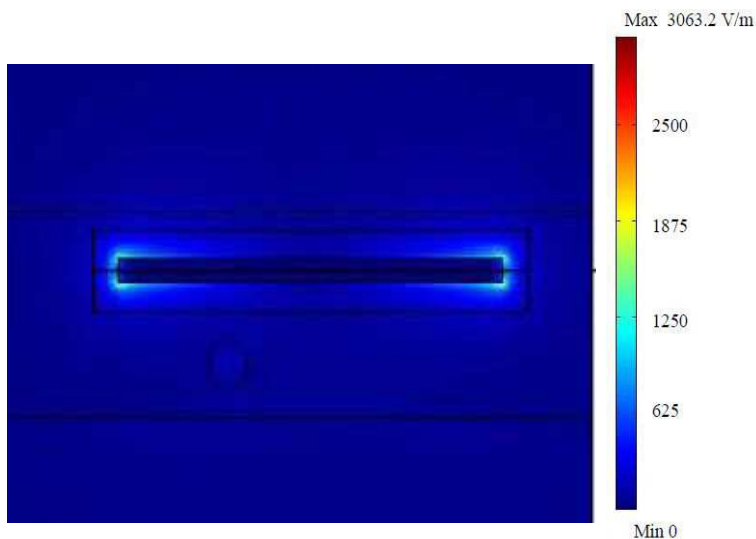
Figure 1. Spatial electric field distribution around the 15 cm long stent implant. The implant is the inner cylinder with an intense RF electric field around its ends. The outer box is for meshing purposes only. The round mark below the left-half of the stent is an insulation post.
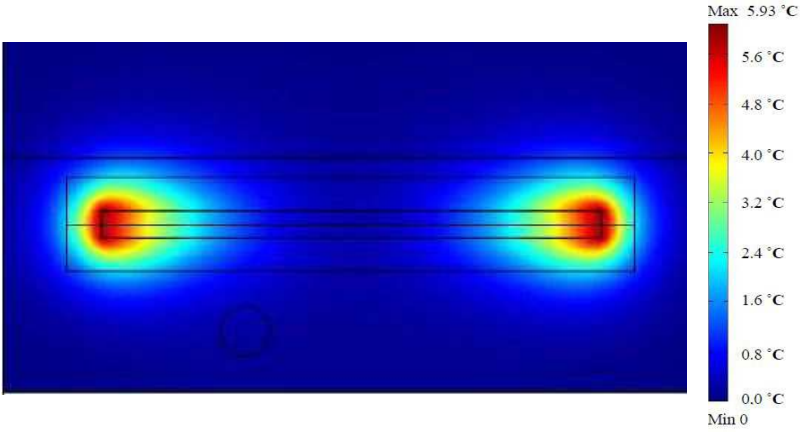
Figure 2. Spatial temperature rise distribution around the stent implant after MR power has been applied for sixteen minutes.
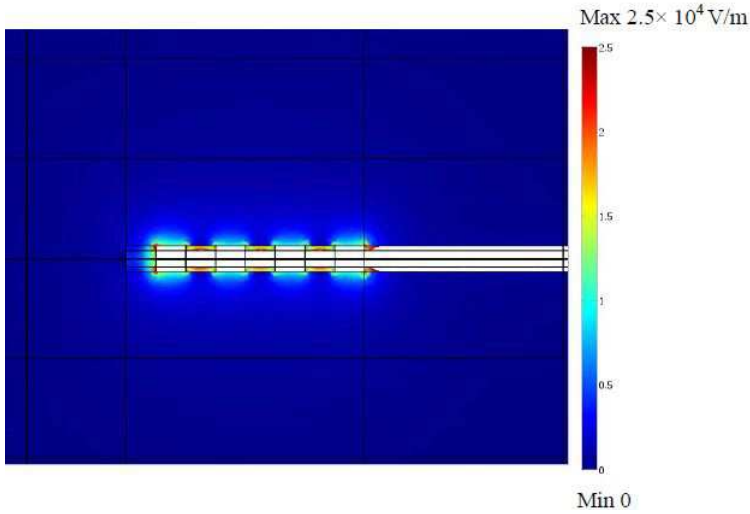
Figure 3. Spatial electric field distribution around the lead implant.

same as those obtained using simplified FEM, there being only a small difference in the overall value. This is best stated quantitatively. Let E be the magnitude of the RF electric field at *any* space point. Then the following is found to hold for the computed values:

$$\left| \frac{E|_{MoM} - E|_{other}}{E|_{MoM}} \right| < 0.03$$
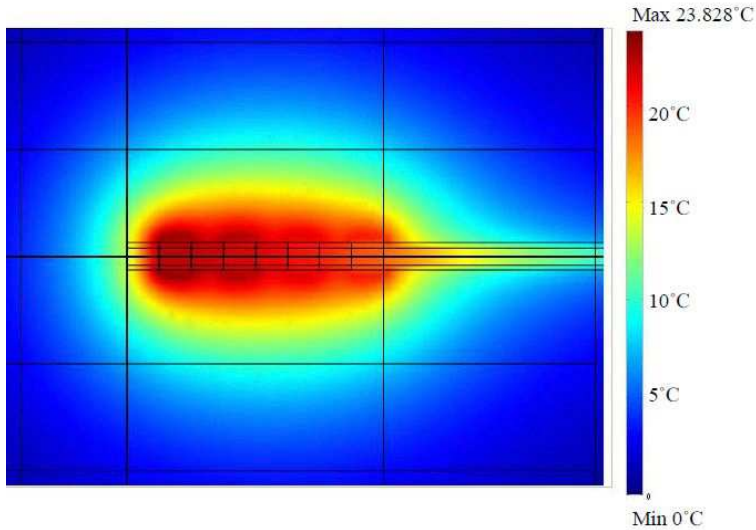
Figure 4. Spatial temperature rise distribution around the lead implant after MR power has been applied for six minutes.

Table 1. Comparisons between the different computed and measured temperature rises. For the stent the values are at a point near the tip and 0.4 mm away from the stent's surface. For the lead, the values are at a point 0.4 mm away from the surface of the proximal electrode. The values of the temperature rise are after MR RF input power has been applied for t (minutes).

Simplified FEM: Temperature rise ($^{\mathrm{o}}$C) after time t (minutes)						Simplified MoM: Temperature rise ($^{\mathrm{o}}$C) after time t (minutes)						Measured temperature rise ($^{\mathrm{o}}$C) after time t (minutes)					
Stent			Lead			Stent			Lead			Stent			Lead		
$t=10$	$t=12$	$t=16$	$t=6$	$t=8$	$t=10$	$t=10$	$t=12$	$t=16$	$t=6$	$t=8$	$t=10$	$t=10$	$t=12$	$t=16$	$t=6$	$t=8$	$t=10$
4.58	5.19	5.64	23.3	24.2	24.8	4.32	4.90	5.32	22.6	23.1	23.5	4.1	4.6	4.9	21.8	22.6	23.0

where the subscript 'other' refers to the simplified FEM or the full FEM. The relation holds at *any arbitrary point* and ensures that the difference in the E field values computed at a point by the various methods is small (less than 3% of the MoM value). Table 1 shows comparisons between the computed and in-vitro measured temperature rises. The measurements were made in the phantom using temperature probes with fiber optic leads. The temperature rises are at a point near the tip of each implant and 0.4 mm from the implant's surface. Each

value is a little less than the spatial maximum which occurs *at* the implant surface.

5. CONCLUSION

The computationally large and expensive problem of the scattering of the MR radiofrequency field by one or more implanted medical devices can be reduced to a simpler one by making some intelligent simplifications in the EM model of the problem. The first simplification is about the MR incident field and the second simplification is about the nonhomogeneous tissue in which an implanted device is embedded. The problem is solved using the simplified EM model and two different numerical techniques, FEM and MoM, are employed. It is found that the computed values agree well with each other as well as with in-vitro measurements made in the laboratory, thus establishing the validity of the simplified EM model. For scattering problems involving other RF sources present near body tissue [19–22] with one or more medical devices implanted in tissue, the model can be used to simplify these problems as well.

ACKNOWLEDGMENT

REFERENCES

1. Amjad, A., R. Kamondetdacha, A. V. Kildishev, S. M. Park, and J. A. Nyenhuis, "Power deposition inside a phantom for testing of MRI heating," *IEEE Trans. Magn.*, Vol. 41, No. 10, 4185–4187, Oct. 2005.

2. Jin, J. M., J. Chen, W. C. Chew, H. Gan, R. L. Magin, and P. J. Dimbylow, "Computation of electromagnetic fields for high-frequency magnetic resonance imaging applications," *Phys. Med. Biol.*, Vol. 41, 2719–2738, 1996.

3. Mohsin, S. A., N. M. Sheikh, and W. Abbas, "MRI induced heating of artificial bone implants," *Journal of Electromagnetic Waves and Applications*, Vol. 23, No. 5–6, 799–808, 2009.

4. Mohsin, S. A., N. M. Sheikh, and U. Saeed, "MRI-induced heating of deep brain stimulation leads," *Phys. Med. Biol.*, 5745–5756, 2008.

5. Mohsin, S. A., U. Saeed, J. Nyenhuis, and N. M. Sheikh, "Interaction of the RF field with stent devices during diagnostic and interventional magnetic resonance imaging," *USNC/URSI National Radio Science Meeting*, San Diego, CA, USA, Jul. 5–12, 2008.

6. Nyenhuis, J. A., S. M. Park, R. Kamondetdacha, A. Amjad, F. G. Shellock, and A. Rezai, "MRI and implanted medical devices: Basic interactions with an emphasis on heating," *IEEE Trans. Device and Materials Reliability*, Vol. 5, No. 3, Sep. 2005.

7. Yeung, C. J., R. C. Susil, and E. Atalar, "RF safety of wires in interventional MRI: Using a safety index," *Magnetic Resonance in Medicine*, Vol. 47, 187–193, 2002.

8. Shellock, F. G., "Magnetic resonance safety update 2002: Implants and devices," *Journal of Magnetic Resonance Imaging*, Vol. 16, 485–496, 2002.

9. Mohsin, S. A., N. M. Sheikh, and U. Saeed, "MRI induced heating of deep brain stimulation leads: Effect of the air-tissue interface," *Progress In Electromagnetics Research*, Vol. 83, 81–91, 2008.

10. Amjad, A., "Specific absorption rate during magnetic resonance imaging," Ph.D. Thesis, Purdue University, 2007.

11. Park, S.-M., R. Kamondetdacha, and J. A. Nyenhuis, "Calculation of MRI-induced heating of an implanted medical lead wire with an electric field transfer function," *Journal of Magnetic Resonance Imaging*, Vol. 26, 1278–1285, 2007.

12. Balanis, C. A., *Advanced Engineering Electromagnetics*, John Wiley & Sons, N.Y., 1989.

13. Harrington, R. F., *Field Computation by Moment Methods*, Wiley-Interscience and IEEE Press Series on Electromagnetic Wave Theory, 1993.

14. Harrington, R. F., *Time-harmonic Electromagnetic Fields*, Chapter 3, New York, McGraw-Hill, 1961.

15. Rumsey, V. H., "Reaction concept in electromagnetic theory," *Phys. Rev.*, Vol 94, No. 6, 1483–1491, 1954.

16. Volakis, J. L., A. Chatterjee, and L. C. Kempel, *Finite Element Method for Electromagnetics*, The IEEE/OUP Series on Electromagnetic Wave Theory, 1998.

17. Jin, J. M., *The Finite Element Method in Electromagnetics*, 2nd edition, John Wiley and Sons, 2002.

18. Mohsin, S. A., N. M. Sheikh, F. Mahmood, and W. Abbas, "General considerations regarding scattering of the MRI RF field by implanted medical devices," *Pakistan Journal of Engineering*

and Applied Sciences, Vol. 6, 17–25, Jan. 2010.

19. Khalatbari, S., D. Sardari, A. A. Mirzaee, and H. A. Sadafi, "Calculating SAR in two models of the human head exposed to mobile phones radiations at 900 and 1800 MHz," *PIERS Online*, Vol. 2, No. 1, 104–109, 2006.

20. Ibrahiem, A., C. Dale, W. Tabbara, and J. Wiart, "Analysis of the temperature increase linked to the power induced by RF source," *Progress In Electromagnetics Research*, Vol. 52, 23–46, 2005.

21. Kouveliotis, K. and C. N. Capsalis, "Prediction of the SAR level induced in a dielectric sphere by a thin wire dipole antenna," *Progress In Electromagnetics Research*, Vol. 80, 321–336, 2008.

22. Kuo, L.-C., Y.-C. Kan, and H.-R. Chuang, "Analusis of a 900/1800-MHz dual-band gap loop antenna on a handset with proximate head and hand model," *Journal of Electromagnetic Waves and Applications*, Vol. 21, No. 1, 107–122, 2007.